

# Development & Validation of a Packed Bed Thermal Energy Storage Model

Javier A. Martell<sup>1,\*</sup> , Luke P. McLaughlin<sup>1</sup> , and Kenneth Armijo<sup>1</sup> 

<sup>1</sup>Sandia National Laboratories

\*Correspondence: Javier Martell, [jamarte@sandia.gov](mailto:jamarte@sandia.gov)

**Abstract.** The rapid growth of economies and population around the world have exponentially increased the demand for energy. This demand has invoked increased annual global CO<sub>2</sub> emissions and necessitated a transition to clean energy technologies. Reliable and affordable energy storage technologies are paramount for increasing renewable energy penetration onto the grid, supporting periods with reduced or no renewable energy generation. This project is aimed at developing a Thermal Energy Storage (TES) solution that can deliver heat to a heat engine for power production or to an industrial process for prolonged periods. TES long duration energy storage (LDES) presents many potential benefits, including 1) Low Cost 2) scalability 3) high energy density 4) low carbon footprint and 5) resiliency via ability to produce synchronous power (i.e., spinning turbomachinery). The broader objective of this project is to build, test, and model the TES concept at a 2 MWh scale to determine the economic and physics-based practicality of the system. The work presented here describes the first phase objectives of the project, including benchtop scale testing, model development, and Model Validation.

**Keywords:** Thermal Energy Storage, Packed Bed, Low Cost, Model Validation

## 1. Introduction

It's widely recognized that carbon dioxide (CO<sub>2</sub>) emissions must be significantly reduced to slow the effects of climate change. In 2022, the U.S. electric power sector emitted 1,539 million metric tons (MMmt) of CO<sub>2</sub>, corresponding to approximately 31% of total U.S. energy-related CO<sub>2</sub> emissions [1]. The growing use of renewable energies such as wind, hydroelectric, solar, biomass and geothermal energy are helping to reduce carbon emissions, but their use is not high enough to achieve decarbonization goals. In 2022, renewable energy sources only accounted for about 13.1% of total U.S. primary energy consumption [2]. One limitation of renewable energy technologies is their intermittency. Coal and natural gas fired energy generation can be steadily produced day and night with no interruption. Renewable technologies like solar and wind suffer from intermittent periods with reduced or no resource available to produce power. With the use of an energy storage system (ESS), this challenge can be overcome.

The need for energy storage development to meet increasing electrification is substantial. An increase from less than 0.5 TWh annual production today to 2 to 10 terawatt-hours (TWh) of annual production is required by 2030 [3]. With the lithium-ion battery as the current dominant storage technology, a key constraint is the limited availability of raw materials, including lithium, cobalt, and nickel [3]. A promising ESS alternative is thermal energy storage (TES). TES can be achieved by storing energy in latent, sensible, and/or thermochemical forms

and later deployed as heat or by converting the stored heat to electricity. TES presents many potential benefits: 1) low cost 2) scalability 3) high energy density 4) low carbon footprint 5) resiliency via ability to produce synchronous power (i.e., spinning turbomachinery). TES can narrow the gap between the global energy demand and the supply in various applications.

The costs associated with building and testing a full-scale ESS prototype necessitate a quick and reliable method to simulate system performance and inform design decisions. By having a "Digital Twin" of an ESS system, decisions regarding the materials and conditions needed to achieve peak efficiency and performance requirements can be made. High fidelity models are needed to confidently make design decisions and understand system physics whereas simple and user-friendly modeling tools are needed to understand general system performance and allow for quick system sizing.

In this work, Sandia National Laboratories (SNL) modeled a TES concept by Planet A Energy (PAE) to develop tools and insights necessary to efficiently design, build, and test a full-scale system. Physics-based 1D and CFD models were developed to capture the physical behavior of the PAE TES system, and models were validated against experimental data sets. A comparison of measured and modeled results is made, and next steps are described.

## 2. Methods

### 2.1. Experimental Test Apparatus

Planet A Energy (PAE) is developing a modular TES system that stores sensible heat in a sand-like material. The system is charged via concentrated sunlight directly without any heat transfer fluid and is discharged by flowing air over the high temperature sand. PAE has developed a small-scale Heat Extraction Testbed to characterize the heat transfer characteristics and inform the full-scale design. The system is currently at Technology Readiness Level (TRL) 4, and Figure 1 shows the testbed concept. The testbed is a 72x30x23 in. rectangular container. The system consists of a packed bed of sand (coal slag), a steel box to store the sand, 6 in. of insulation (nanopore board) to slow heat loss, and electric heaters to heat the sand. The sand height is half the height of the steel box, and the box has two 2.5 in. circular openings above the sand on opposite ends of the box to allow for airflow over the top of the sand.



**Figure 1.** Planet A heat extraction testbed concept.

Three operational states are considered: 1) charge – resistive heaters located below the sand apply a total power input of 700W for 7hr (4.9 kWh). 2) hold – stop electric heating and allow the system to rest for 10 hours. 3) discharge – air is flowed over the sand at a rate of 12 LPM for 15hr. Thermocouples are placed throughout the packed bed at different locations, depths, and heights to measure the storage media temperature. Figure 2 indicates the thermocouple locations within the packed bed.

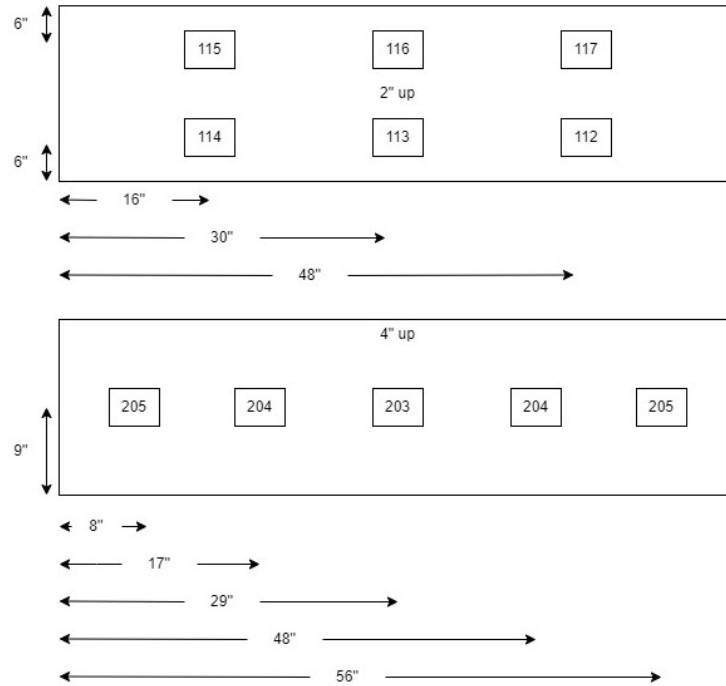


**Figure 2.** Top/down view of thermocouples placement 2" up (upper) and 4" up (lower) from bottom of sand.

## 2.2. Modeling

### 2.2.1. CFD Modeling

The PAE TRL 4 Test Bed was assessed via CFD using ANSYS Fluid Flow (Fluent with Fluent Meshing) solver. The modeled geometry consists of three solid regions: 1) steel box, 2) insulation, and 3) sand – and one fluid region. The system geometry was simplified from the full fidelity design to reduce computational cost. An example of geometry simplification is shown in Figure 3. The fluid region was created by enclosing the inlet and outlet portion of the model. The meshing was done using a min and max size of 0.001 and 0.005 m, respectively. An example mesh is found in Figure 4. Mesh inflation was applied at the inlet and outlet of the bed. The total number of cells for the mesh are 4,341,427 with a maximum skewness of 0.5732.

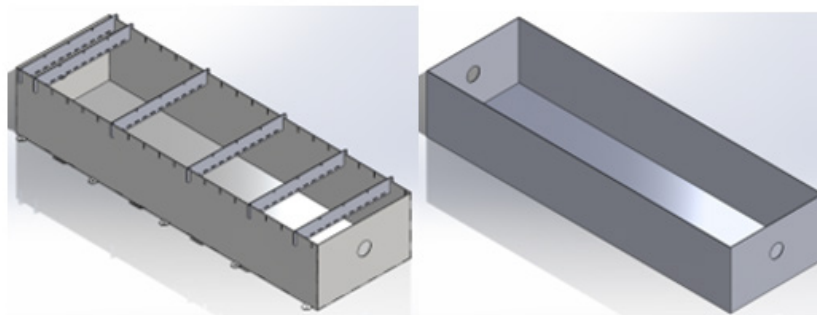


**Figure 3.** Steel box (left) and steel box simplification (right) CAD model.

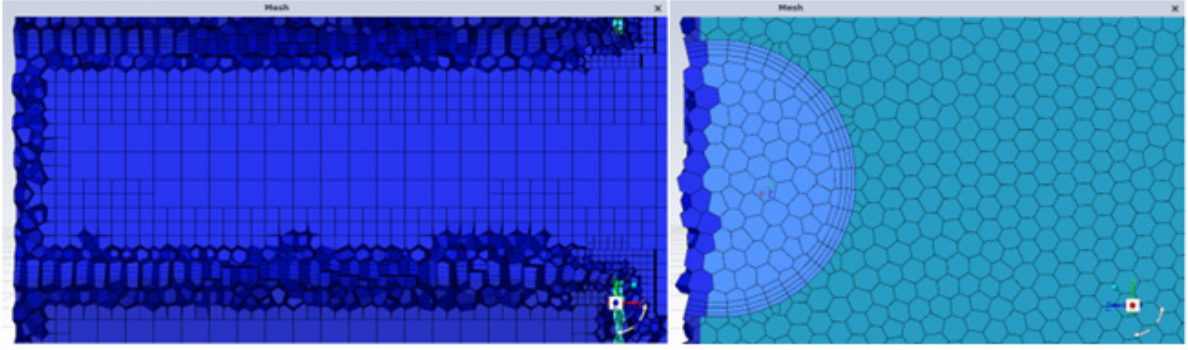


Figure 4. Cross section view (left) and inlet inflation (right) mesh.

### 2.2.1.1. Packed Bed Surface Flow

The physics to model the surface flow system are captured using the Ansys “energy equation” model. Radiative heat transfer within the system was not modeled to reduce computational expense. Ansys Fluent solves the energy equation in the following form:

$$\frac{\partial}{\partial t} \left( \rho \left( e + \frac{v^2}{2} \right) \right) + \nabla \cdot \left( \rho v \left( h + \frac{v^2}{2} \right) \right) = \nabla \cdot \left( k_{eff} \nabla T - \sum_{j,j_j} \tau_{eff}^j \cdot \underline{v} \right) + S_h \quad (1)$$

The first three terms on the right-hand side represent energy transfer due to conduction, species diffusion, and viscous dissipation, respectively. In this case, only conduction is being considered in the system. Laminar flow was assumed in the system for computational efficiency purposes. The materials used for this model are air, steel, sand, and insulation, and their properties are tabulated in Table 1. A convective heat transfer condition was applied to the outer system walls to capture heat loss from the system. A value of 5 W/(m<sup>2</sup>K) was used as the heat transfer coefficient with an ambient free stream temperature of 25°C.

Table 1. Material Properties

Material	Density [kg/m <sup>3</sup> ]	Cp [J/(Kg K)]	Thermal Conductivity [W/(m K)]	Viscosity [Kg/(m s)]
Air	1.23	1006.43	0.024	1.79e-05
Steel	803	502.48	16.27	N/A
Sand	1,500	800	0.2	N/A
Insulation	15	1,200	0.04	N/A

A heat flux of 1032 W/m<sup>2</sup> (700 W) was added to the bottom sand surface during the “charge” phase. The phase was run for 100 steps with a time step size of 252 s. For the second phase (hold), the heat flux was removed, and the system was let to rest. The case was run for 100 steps with a time step of 360 s. For the third state (discharge), a mass flow rate of 0.000233 kg/s (12LPM) at a temperature of 25 °C was applied at the inlet of the system. A temperature of 250 °C was applied to the sand prior to the discharge phase to allow for comparison with the experimental data. The experimental discharge was performed at a different time than the charge and hold phases where only the discharge data was recorded. The case was run for 100 steps with a time step of 540 s. A complete charge-hold-discharge experimental data set will be assessed in the next phase of the project.

### 2.2.1.2. Packed Bed Through Flow

A second CFD model was created to compare system performance when the discharge air flows through the packed bed rather than over the surface. To model the flow through the packed bed, the ANSYS model was adapted to a porous media model and the sand storage

media was replaced with gravel to increase porosity. The conduction flux and the transient terms from Equation (1) to Equation (2) were modified. The viscous resistance and inertial resistance associated with the porous media model were specified using Equations (3) and (4), respectively.

$$\frac{\partial}{\partial t}(\gamma\rho_f E_f + (1-\gamma)\rho_s E_s) + \nabla \cdot (\underline{v}(\rho_f E_f p)) = \nabla \cdot [k_{eff} \nabla T - (\sum h_i j_i) + (\underline{\tau} \cdot \underline{v})] + S_f^h \quad (2)$$

$$\alpha = \frac{D_p^2}{150} \cdot \frac{\varepsilon^3}{(1-\varepsilon)^2} \quad (3)$$

$$C_2 = \frac{3.5}{D_p} \cdot \frac{(1-\varepsilon)}{\varepsilon^3} \quad (4)$$

A gravel particle diameter ( $D_p$ ) of 0.002 m and porosity ( $\varepsilon$ ) of 0.25 were applied. The viscous and inertial resistances were determined to be 1.35E+09 and 84,000, respectively. Table 2 shows the material properties for gravel. Because the specific heat of the sand and gravel medias varied by only 5%, the porous media masses were set to equal that of the surface flow model to compare a system with similar energy storage capacity. The heat flux boundary conditions applied to the surface flow model were also applied to the through flow model.

**Table 2.** Gravel material properties.

<b>Density [kg/m<sup>3</sup>]</b>	1,840
<b>Cp [J/(Kg K)]</b>	840
<b>Thermal Conductivity [W/(m K)]</b>	0.36

## 2.2.2. 1D Modeling

In addition to high fidelity CFD modeling, this study presents a simplified computational approach to model the thermal behavior of the PAE surface flow TES system. A pseudo-steady state one-dimensional framework was chosen to simplify the assessment approach and enable rapid computations. Here, heat transfer is assessed along the axial direction of the TRL 4 test bed. To achieve this, a resistive heat transfer network is employed to quantify heat loss from the system, wherein nodes represent spatial elements within the system. The resistive network for a surface flow model during a charge and hold is shown in Figure 5. These nodes incorporate resistances to account for parallel conduction through the sand and surface air, conduction through the system insulation and outer shell, and convection at the outer surface. The heat loss rate of the system at each time step is realized following Equation 5 where  $T_s$  is the bulk sand & air temperature inside the testbed,  $T_f$  is the free stream external temperature,  $t$  is the respective material thickness,  $k$  is the respective material thermal conductivity,  $A_{CS}$  is the respective material axial cross section area,  $A_{SA}$  is the external surface area, and  $h$  is the external convective heat transfer coefficient. Subscripts s, a, i, and o represent sand, air, insulation, and outer shell material, respectively. The pseudo-steady analysis scheme is deployed using Equation 6 where  $Q_{in}$  is the energy into the system,  $Q_{out}$  is the energy out of the system, and  $m_{sys}$  is the system mass.

$$Q_{out} = \frac{T_s - T_f}{\left(\frac{k_s A_{CS_s} + k_a A_{CS_a}}{t_s} + \frac{k_i A_{CS_i}}{t_i}\right) + \left(\frac{t_o}{k_o A_{CS_o}}\right) + \left(\frac{1}{h A_{SA}}\right)} \quad (5)$$

$$T_s^{j+1} = T_s^j + \frac{Q_{in} - Q_{out}}{m_{sys}} \quad (6)$$

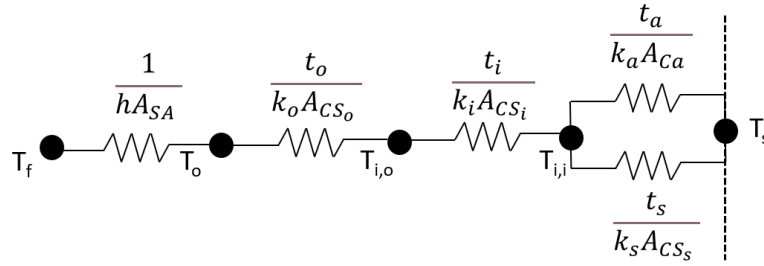


Figure 5. Surface flow model resistive network.

While this 1D numerical model offers valuable insights into the transient thermal response of insulated boxes containing granular materials, it is important to acknowledge its limitations. The 1D model's simplicity provides a practical and computationally efficient tool for initial analyses, enabling rapid assessments of system behavior. However, it does not capture complex and multi-dimensional physical phenomena that could be significant in more intricate scenarios. For instance, it does not account for internal natural convection or radiative heat transfer. Additionally, any three-dimensional effects, such as temperature gradients across the width or height of the box, are not considered within this 1D framework. Therefore, for situations where these factors are critical, the more detailed and comprehensive CFD modeling approach will be warranted.

### 3. Results

#### 3.1. Comparison between experimental, CFD and 1D model

Figure 6 shows experimentally measured sand temperatures at different bed locations as a function of test time. The temperature was taken every minute for the duration of the experiment. To simplify the comparison of experimental and simulated results, experimental thermocouple temperatures were averaged and compared to the CFD and 1D model average media temperatures as a function of test time, and this result is shown in Figure 7.

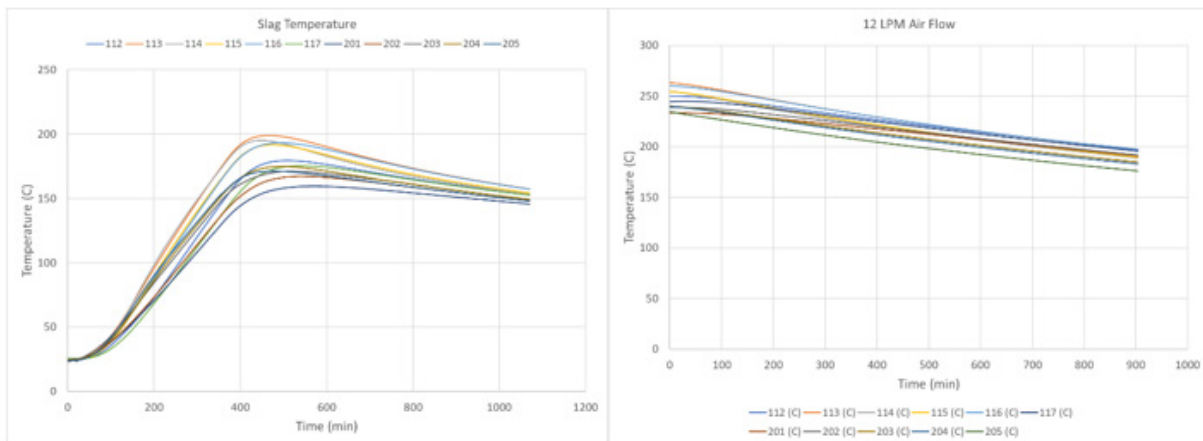
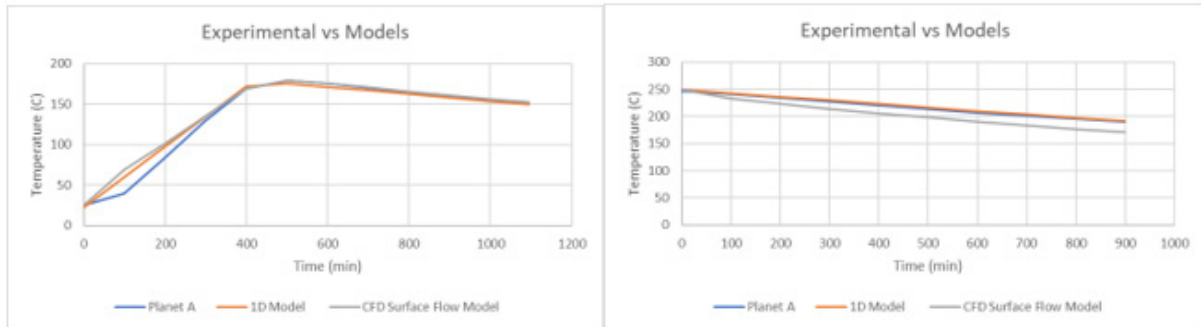


Figure 6. Experimental data plot for charge, hold (left) and discharge (right).

After the charge state was completed, the experimental average temperature of the sand reached 173.46°C with an average temperature increase of 0.35°C/min. After the hold state, the average temperature was 151.09°C, with an average cool down of 0.033°C/min. Charge/hold and discharge experiments were run separately. Discharge experiments were started after the bed reached a steady state temperature of 250 °C. After the discharge the average temperature was 189.98°C with an average cool down of 0.063°C/min.

The results for the CFD surface flow model in ANSYS Fluent are compared to the experiments in Figure 7. After charge, the average temperature of the sand was 174.99°C with an average temperature increase of 0.36°C. After hold, the average temperature was 152.06°C with an average cool down of 0.034°C. After discharge, the average temperature was 170.31°C with an average cool down of 0.089°C.

The 1D model results are also compared to the experiments as well as the CFD model in Figure 7. After charge, the average temperature of the sand was 179.09°C with an average temperature increase of 0.37°C/min. After hold, the average temperature was 149.77°C with an average cool down of 0.044°C/min. After discharge, the average temperature was 191.30°C with an average cool down of 0.065°C/min.



**Figure 7.** Comparison between experimental and models data.

Tables 3 and 4 compare the measured and modeled rate of temperature change in the storage media and the final storage media temperatures at the end of each operational state, respectively. The CFD and 1D models well capture the behavior of the experimental system, with the CFD model having the highest accuracy. The percent errors in Table 3 are higher compared to Table 4, but this does not mean that the models are unreliable. Small variations in simulated and measured rates of temperature change result in large percent errors. On the contrary, the absolute temperatures of the storage media at the end of each cycle compare within much smaller percent errors. The finding suggests it is important to consider prediction errors on both an absolute temperature and rate of temperature change basis to fully capture the suitability of the models.

It can be observed from Figure 7 that the simulated storage media temperatures increase at a faster rate over the first 100 minutes of charging compared to the experiments. Simulated temperatures increase at a nearly constant rate throughout the entirety of charging whereas experimental heating accelerated after 100 minutes. Notably, experimental and simulated temperatures converged by the end of charging within 2.07% of experimental data. Variation in experimental and simulated heating rates is partially contributed to by the applied heating boundary conditions. The models assume that the entirety of the bottom face is heated uniformly whereas the experimental setup has spatial discontinuities in applied heat and regions with no heating at all. During holding, the measured and simulated temperatures decrease at a similar rate, converging within 0.76% of experimental data. For the discharge phase, the 1D model and the experimental data converged almost exactly within 0.69%. The CFD model had a higher divergence during discharge, but this may be due to the 20 iterations that the model took to converge. A smaller time step and an increase in steps can help achieve better convergence and may improve results.

**Table 3.** Rate of temperature change between models and data.

Phase	PAE Data (°C/min)	1D Model (°C/min)	CFD Model (°C/min)	1D Model %Error	CFD Model % Error
Charge	0.35	0.37	0.36	5.71	2.86
Hold	-0.033	-0.044	-0.034	33.33	3.03
Discharge	-0.063	-0.065	-0.084	3.17	33.33

**Table 4.** Final temperature comparison between states.

Phase	PAE Data (°C)	1D Model (°C)	CFD Model (°C)	1D Model %Error	CFD Model % Error
Charge	173.46	179.09	174.99	3.25	0.88
Hold	151.09	149.77	152.06	0.87	0.64
Discharge	189.98	191.30	170.31	0.69	10.35

### 3.2. Comparison between packed bed surface and through flow

The CFD surface flow model results were compared to those from the CFD through flow model to elucidate differences in system performance. Specifically, differences in system discharge behavior are highlighted here. Figure 8 compares the CFD derived media temperatures of the surface flow and through flow models over the discharge phase. The through flow model is observed to remove heat from the media at a faster rate than the surface flow model. At the end of discharge, the through flow model achieved a final media temperature near 60 °C while the final temperature of the surface flow model was near 170 °C. This result is attributed to 1) an improved heat transfer coefficient when flowing the heat transfer fluid through the media rather than over the media and 2) significantly increased heat transfer surface area in the flow through scenario.

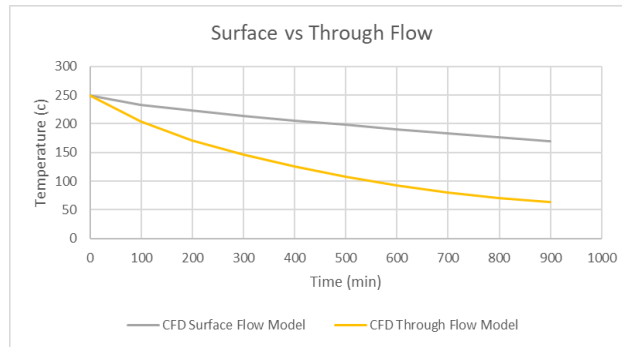


**Figure 8.** Comparison between surface and through flow model discharge.

Round-trip efficiency (RTE) was assessed for both system designs following Equation 7 where  $E_{out}$  is the energy extracted from the system during discharge and  $E_{in}$  is the energy input to the system during charging. The energy input to both systems was 4.9 kWh. The energies extracted from the surface and through flow models were 0.27 kWh and 1.044 kWh, respectively. The surface flow model had a RTE of 5.51% and the through flow model had a RTE of 21.31%. Although both models do not show a high efficiency, it is important to note that this efficiency is associated with a small-scale test system and was calculated for a fixed 15hr discharge. Increasing system size will improve system efficiency by increasing the volume-to-surface area ratio of the storage system, reducing the relative amount of energy lost from the storage system. Furthermore, a deeper discharge of each system would enable increased energy extraction and increase the system efficiency. It is noted, however, that the exergy associated with the energy extracted at the end of discharge is low. The minimum

discharge level of the system will be dictated by the downstream process requirements, i.e., power and temperature.

$$RTE = \frac{E_{out}}{E_{in}} \quad (7)$$

## 4. Conclusions

Sandia National Laboratories (SNL) modeled a TES concept by Planet A Energy (PAE) to develop tools and insights necessary to design, build, and test a full-scale system. 1D and CFD models were developed and validated against experimental data sets, enabling cost-effective means for large-scale system design and performance assessments. The 1D model, having an average prediction error of 7.43%, allows for quick and user-friendly analysis of the storage system, offering scenario-specific simulations and future techno economic modeling with hourly resolution over extended periods. Meanwhile, the high-fidelity CFD model, with an average percent error of 8.05%, provides a deeper dive into the physical behavior of the system, including multi-dimension thermal gradients, localized regions of heat loss, and thermally induced mechanical stresses. Furthermore, the CFD model enabled comparison between surface flow and through flow discharge scenarios, enabling a precise evaluation of efficiency and suitability for various applications. This integrated modeling approach paves the way for the development of higher Technology Readiness Level (TRL) systems, leveraging the strength of both models to continuously enhance accuracy and performance with each iteration.

Project next steps include the development, testing, and modeling of a 2 MWh (TRL6) PAE TES system. The models validated in this work will be used to optimize the TRL 6 system design, including insulation thickness, packed bed packing density, and discharge heat transfer fluid mass flow rate. The TRL 6 system will be charged using CSP technologies rather than electrical heating, and the system will be tested at Sandia National Laboratories. The TRL 6 system will serve as a demonstration of the system efficacy for future industry applications.

## Data availability statement

The data presented in this work is protected under a collaboration agreement between Sandia National Laboratories and Planet A Energy. Data availability can be sought by contacting Luke McLaughlin of Sandia National Laboratories and Brad Hines of Planet A Energy.

## Author contributions

Javier Martell is credited with writing the manuscript, performing CFD simulations, and data analysis. Luke McLaughlin is credited with project management, manuscript review, 1D modeling, and data analysis. Kenneth Armijo is credited with project management and manuscript review.

## Competing interests

The Authors declare no competing interests.

## Funding

This project was funded by a U.S. Department of Energy AOP Project under CPS Agreement # CPS38895

## Acknowledgement

Sandia National Laboratories is a multi-mission laboratory managed and operated by National Technology & Engineering Solutions of Sandia, LLC, a wholly owned subsidiary of Honeywell International Inc., for the U.S. Department of Energy's National Nuclear Security Administration under contract DE-NA0003525.

## References

1. "How much of U.S. carbon dioxide emissions are associated with electricity generation?". U.S. Energy Information Administration. <https://www.eia.gov/tools/faqs/faq.php?id=77&t=11> (09/18/23)
2. "How much of U.S. energy consumption and electricity generation comes from renewable energy sources?" U.S. Energy Information Administration. <https://www.eia.gov/tools/faqs/faq.php?id=92&t=4#:~:text=How%20much%20of%20U.S.%20energy,total%20utility%2Dscale%20electricity%20generation> (09/16/2023)
3. C. Julie. "Turning Up the Heat: Thermal Energy Storage Could Play Major Role in Decarbonizing Buildings." Berkely Lab. <https://newscenter.lbl.gov/2021/11/18/turning-up-the-heat-thermal-energy-storage-could-play-major-role-in-decarbonizing-buildings/> (09/15/2023)